药 食 同 源 资 源
FOOD & MEDICINE HOMOLOGY RESOURCES
ISSN 3136-103X (online)
https://doi.org/10.26599/FMHR.2026.9740012

Research Article

Multi-omics analysis reveals the rules of component transformation and the mechanism of quality formation of *Phyllanthi Fructus* during natural sun-drying process

Hao-Zhou Huang[1, †], Meng-Qi Li[2, †], San-Hu Fan[3], Tai-Gang Mo[3], Ding-Kun Zhang[1, 4] (✉), Li Han[1] (✉), Jun-Zhi Lin[5] (✉)

[1] *Chinese Medicine Germplasm Resources Innovation and Effective Uses Key Laboratory of Sichuan Province, State key Laboratory of Southwestern Chinese Medicine Resources, School of Modern Chinese Medicine Industry, Chengdu University of Traditional Chinese Medicine, Chengdu* 611137, *China*

[2] *Pharmacy department, Sichuan Nursing Vocational College, Chengdu* 610100, *China*

[3] *Sanajon Pharmaceutical Group, Chengdu* 610000, *China*

[4] *Sichuan Provincial Engineering Research Center of Innovative Re-development of Famous Classical Formulas, Tianfu TCM Innovation Harbour, Chengdu University of Traditional Chinese Medicine, Pengzhou* 611900, *China*

[5] *TCM Regulating Metabolic Diseases Key Laboratory of Sichuan Province, Hospital of Chengdu University of Traditional Chinese Medicine, Chengdu* 610072, *China*

[†] *Hao-Zhou Huang and Meng-Qi Li contributed equally to this work.*

Received: 17 August 2026 / **Revised:** 26 August 2026 / **Accepted:** 16 September 2026

Abstract: Natural sun-drying facilitates quality formation of *Phyllanthi Fructus* (PF) *via* enhanced accumulation of bioactive constituents. Nevertheless, its underlying molecular regulatory mechanisms remain poorly understood, which impedes standardized quality control for this medicinal herb. In this study, transcriptomic and metabolomic approaches were integrated to systematically investigate time-course alterations in gene expression and metabolite abundance throughout an 11-day natural sun-drying process. Microstructural observations demonstrated that PF fruit cells retained intact morphological structures during the first four drying days, suggesting potential stress-triggered physiological responses. Key bioactive compounds such as gallic acid, chebulagic acid, ellagic acid and punicalagin gradually accumulated and peaked on day 8 of sun-drying. Transcriptome analysis identified 2,515 differentially expressed genes (DEGs), with 1,261 up-regulated and 1,254 down-regulated transcripts. Functional enrichment showed these DEGs were principally enriched in three secondary-metabolism-related pathways: Phenylpropanoid biosynthesis (53 DEGs), flavone and flavonol biosynthesis (8 DEGs), and terpenoid backbone biosynthesis (23 DEGs). Metabolomics further annotated 58 differential metabolites largely involved in unsaturated fatty acid biosynthesis, the tricarboxylic acid (TCA) cycle, as well as flavonoid biosynthesis. These metabolic pathways are tightly linked to plant adaptive responses to combined dehydration-heat stress during post-harvest sun-drying.

The present results demonstrate that drought and heat stress generated during natural sun-drying processing are capable of triggering secondary metabolism, promoting the enrichment of bioactive compounds and elevating the medicinal quality of PF, which lays a solid scientific foundation for the optimization of processing strategies and formulation of quality evaluation criteria.

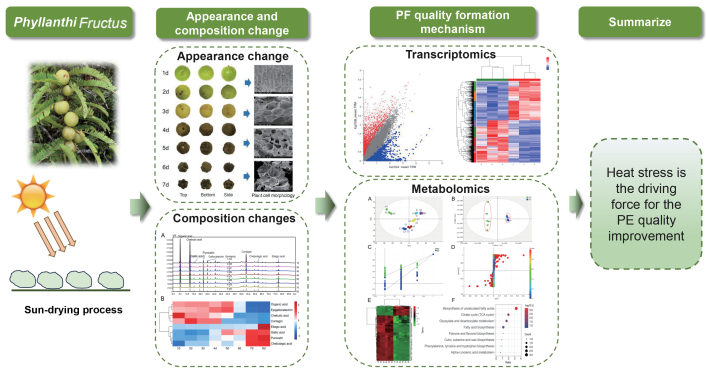

Keywords: *Phyllanthi Fructus*; heat stress; sun-drying; polyphenol; transcriptomics; metabolomics; quality formation

Citation: Huang H. Z., Li M. Q., Fan S. H., et al. Multi-omics analysis reveals the rules of component transformation and the mechanism of quality formation of *Phyllanthi Fructus* during natural sun-drying process. *Food & Medicine Homology Resources*, 2026, 1: 9740012. https://doi.org/10.26599/FMHR.2026.9740012

© National R & D Center for Edible Fungus Processing Technology, China 2026. Published by Tsinghua University Press. This is an open access article under the CC BY-NC-ND license (http://creativecommons.org/licenses/by-nc-nd/4.0/).

Address correspondence to Ding-Kun Zhang, zhangdingkun@cdutcm.edu.cn; Li Han, hanliyx@163.com; Jun-Zhi Lin, 582097013@qq.com

1 Introduction

Phyllanthi Fructus (PF), the mature fruit of *Phyllanthus emblica* L. (Euphorbiaceae), is a well-documented medicinal and edible plant widely cultivated across Southeast Asia and Southwest China[1]. PF accumulates abundant tannins (accounting for up to 33% of its dry weight), phenolic acids, flavonoids and terpenoids, which endow this herb with prominent antioxidant, anti-inflammatory, hepatoprotective and hypoglycemic bioactivities[2-5]. Accordingly, it has been extensively applied in multiple traditional medical systems, including Ayurveda, Tibetan medicine and traditional Chinese medicine (TCM)[6]. Given its outstanding nutritional and therapeutic potentials, the World Health Organization (WHO) has designated PF as one of three prioritized medicinal species for large-scale cultivation[7].

Postharvest drying constitutes an indispensable processing procedure that drastically reshapes the chemical composition and medicinal quality of herbal medicines[8]. Rational selection of drying regimes and precise manipulation of drying parameters lay a solid foundation for quality regulation of medicinal plants[9]. Existing phytochemical evidence has illustrated that postharvest drying essentially imposes severe thermal and dehydration stress on plant tissues[10]. Secondary metabolites, the core bioactive constituents of herbal materials, are generally biosynthesized and accumulated in response to fluctuating temperature and humidity stresses. A representative example is ginseng, whose ginsenoside levels rise markedly throughout field harvesting and natural sun-drying[11]. Previous research has reported that fresh PF fruits contain less than 0.4% gallic acid, a concentration insufficient to meet official quality criteria; nevertheless, sun-drying dramatically elevates gallic acid and other polyphenol derivatives in PF[7]. Such observations imply that sun-drying stress activates secondary metabolic cascades in PF, facilitating the conversion of precursor substances into bioactive polyphenols. Nevertheless, the dynamic transformation rules of metabolites, the core molecular regulatory networks, and the critical stress factors governing quality promotion remain largely uncharacterized. This unresolved scientific bottleneck further leads to inconsistent quality among PF batches, restricting the standardized production and sustainable exploitation of this medicinal herb.

To fill these research gaps, the current study combined transcriptomics and UPLC-QTOF-MS-based untargeted metabolomics to achieve four research objectives: (1) characterize temporal variations in tissue microstructure, moisture content and major bioactive compounds during an 11-day natural sun-drying period; (2) screen differentially expressed genes (DEGs) and core metabolic pathways participating in stress adaptation and secondary metabolite biosynthesis; (3) annotate differential metabolites and map their corresponding metabolic routes; (4) integrate multi-omics datasets to decode the molecular regulatory cascade connecting sun-drying stress and quality improvement in PF. To our knowledge, this study delivers the first systematic multi-omics dissection of postharvest processing in PF. The obtained results not only interpret the molecular rationale behind the conventional sun-drying processing technique, but also supply candidate molecular biomarkers and optimized processing parameters (e.g., 8 days of sun exposure) for PF quality evaluation and standard formulation.

2 Instruments and materials

2.1 Instruments

The instruments include a Shimadzu LC-20AT high performance liquid chromatograph (Shimadzu Corporation, Japan), Milli-Q ultrapure water system (Millipore Corporation, USA), Sartorius BT25S analytical balance and Sartorius BSA224S analytical balance (Sartorius AG, Germany), KQ-500DE numerical control ultrasonic cleaner (Kunshan Ultrasonic Instruments Co., Ltd.). The Scientz-10N/C freeze dryer (Ningbo Scientz Biotechnology Co., Ltd.), a NanoDrop 2000 spectrophotometer (Thermo Scientific, USA), an electrophoresis apparatus (DYY-6C model, Beijing Liuyi Instrument Factory), and an agarose gel horizontal electrophoresis tank (DYCP-31F, Beijing Liuyi Instrument Factory) were used. The Eppendorf MixMate homogenizer (PBC-115353, Eppendorf, Germany) was also included, alongside TRIzol Reagent for animal and microbial RNA extraction kits (Invitrogen, CA), Plant RNA Purification Reagent for plant tissue RNA extraction kits (Invitrogen, CA), a magnetic stand for mRNA separation (Invitrogen, CA), the TruSeq RNA Sample Preparation Kit (Illumina, USA), the Quantus™ Fluorometer (Promega, USA), and the QuantiFluor® dsDNA System (Promega, USA). The Agencourt AMPure XP library purification kit (Beckman Coulter, USA), HiSeq X Reagent Kits (Illumina, USA), and NovaSeq Reagent Kits (Illumina, USA) completed the list of materials used in this study.

2.2 Reagents

Methanol and formic acid (chromatographic grade); the reference standards include gallic acid (batch number 4051109, purity ≥ 98%), epigallocatechin gallate (batch number PRF7072601, purity ≥ 98%), epigallocatechin (batch number 14092403, purity ≥ 98%), catechin (batch number 14051602, purity ≥ 98%), epigallocatechin-3-gallate (batch numbers PRF805242 and PRF15121022, both with purities ≥ 98%), corilagin (batch number PRF7102406, purity ≥ 98%), ellagic acid (batch number PRF7101305, purity ≥ 98%), and chebulic acid (batch number AP8070902, purity ≥ 98%), provided by Chengdu Purifa Technology Development Co., Ltd.; chebulagic acid (batch number CHB171222, purity ≥ 98%), chebulinic acid (batch number CHB171226, purity ≥ 98%), ferulic acid (batch number CHB180206, purity ≥ 98%), ethyl gallate (batch number CHB171109, purity ≥ 98%), and punicalin (batch number CHB170606, purity ≥ 98%) were provided by Chengdu Cloma Biotechnology Co., Ltd.

2.3 Sample collection and preparation

The medicinal materials were collected from Chuxiong in Yunnan Province and identified by Professor Zhang Dingkun from the Chengdu University of TCM as the mature fruit of PF from the Euphorbiaceae family (Table 1). After collection, extraneous tissue parts were excised from the samples. All experimental apparatus and containers were subjected to RNase-free treatment. The surface of the harvested samples was disinfected with ethanol, and then the samples were immediately immersed in liquid nitrogen for rapid freezing. Subsequently, they were stored in a −80 °C ultra-low temperature freezer. The remaining samples were subjected to natural sun-drying. Samples were collected on the fourth day before and after air-drying (as it was determined that beyond this point, it was not feasible to obtain adequate transcriptome samples), which were designated as samples A and B for the pre- and post-sun-drying time points, respectively. Each time point was represented by three biological replicates, employing a total of six samples for the extraction of total RNA and the construction of libraries.

Freeze drying was required before preparing metabolomics samples. The remaining processing methods were consistent with

Table 1 Sample information of PF

Number	Collection location	Source	Altitude (m)
M1	Chuxiong Prefecture, Yunnan	*Phyllanthus emblica* L.	1,900
M2	Chuxiong Prefecture, Yunnan	*Phyllanthus emblica* L.	1,900
M3	Chuxiong Prefecture, Yunnan	*Phyllanthus emblica* L.	1,800
M4	Yuanmou, Yunnan	*Phyllanthus emblica* L.	1,800
M5	Yongren, Yunnan	*Phyllanthus emblica* L.	1,600
M6	Yongren, Yunnan	*Phyllanthus emblica* L.	1,600

those described above, with sampling carried out over 11 days, labeled sequentially from A to K, at intervals of one day, and sample names corresponding to A, C, E, G, I, and K. Each time segment was represented by three biological sample replicates. On the first and eleventh days, the number of biological replicates was increased to six.

2.4 Chromatographic conditions

The chromatographic column used was a Welchrom C18 column (4.6 mm × 250 mm, 5 μm). The mobile phase consisted of 0.2% phosphoric acid in water-methanol. Employing gradient elution, the elution program was as follows: 0–6 min, 5% methanol; 6–15 min, 5% to 7% methanol; 15–20 min, 7% to 15% methanol; 20–25 min, 15% to 21% methanol; 25–31 min, 21% to 22% methanol; 31–41 min, 22% methanol; 41–47 min, 22% to 28% methanol; 47–51 min, 28% to 32% methanol; 51–57 min, 32% to 38% methanol; 57–70 min, 38% to 45% methanol; 70–80 min, 45% to 65% methanol. The detection wavelength was set at 273 nm, with a flow rate of 1.0 mL/min. The column temperature was maintained at 25 °C, and the injection volume was 10 μL[4].

2.5 Drying parameter calculation method

Weigh medicinal herbs at different drying time periods and calculate drying parameters. Calculate the dry basis moisture content (M_t) according to the formula 1.

$$M_t = \frac{W_t - G}{G} \quad (1)$$

In the formula, W_t is the total mass (g) at any drying time t; G is the dry matter mass (g). Drying rate (D_R) shall be calculated according to the formula 2.

$$D_R = \frac{Mt_1 - Mt_2}{t_1 - t_2} \quad (2)$$

In the formula, M_{t1} is the dry basis moisture content ($g \cdot g^{-1}$) at the moment t_1; Mt_2 is the dry basis moisture content ($g \cdot g^{-1}$) at time t_2.

2.6 Sample preparation

2.6.1 *Preparation of reference solutions*

Accurately weigh appropriate amounts of each reference substance and dissolve in 50% methanol aqueous solution to prepare solutions containing gallic acid at 25 μg/mL, epigallocatechin gallate at 62 μg/mL, epigallocatechin at 36 μg/mL, catechin at 20 μg/mL, epigallocatechin-3-gallate at 92 μg/mL, corilagin at 132 μg/mL, ellagic acid at 116 μg/mL, chebulic acid at 104 μg/mL, chebulagic acid at 42 μg/mL, chebulinic acid at 52 μg/mL, ferulic acid at 32 μg/mL, ethyl gallate at 32 μg/mL, and punicalin at 61 μg/mL.

2.6.2 *Preparation of the test solution*

PF samples are naturally sun-dried for approximately 8 days, with daily samples collected and stored at −20 °C until use. After freeze-drying and pulverization to a fine powder (sieved through a No. 3 sieve), take approximately 0.1 g of the sample powder that has been sieved through a No. 3 sieve and accurately weigh it. Place the sample in a capped conical flask, then accurately add 50 mL of 50% methanol aqueous solution. After ultrasonic extraction, allow it to cool, replenish the lost weight, shake well, and filter through a 0.22 μm microporous membrane to obtain the test solution.

2.7 Scanning electron microscopy (SEM) conditions

Take an appropriate amount of tissue from the PF sample and fix it with double-sided conductive adhesive on the sample stage. After gold sputtering, observe the sample using SEM with an accelerating voltage of 15 kV and a working distance of 4.8–5.0 mm, and an emission current of 130–135 mA. The DM2500 microscope (Leica Microsystems, Germany) is equipped with a DP73 type CCD for image capture and computer-assisted image analysis system for completing the microscopic observations.

2.8 Transcriptome experimental methods

2.8.1 *Sequencing experimental procedure*

The present experiment was conducted on the HiSeq platform, which enabled the sequencing of all mRNA transcripts derived from specific tissues of eukaryotes at a particular time point. In this experiment, the Illumina TruSeqtm RNA sample prep Kit was employed for library construction. The operational steps were as follows: (1) Total RNA was extracted. (2) mRNA was enriched. (3) The mRNA was fragmented. (4) Reverse transcription to cDNA was carried out. (5) Adaptor ligation was performed. (6) Illumina sequencing was finally implemented.

2.8.2 *RNA extraction*

Total RNA from the samples was extracted using the TRIzol reagent (Invitrogen), followed by DNA removal with DNase I (Takara). RNA quality was assessed using the 2100 Bioanalyzer (Agilent) and the ND-2000 spectrophotometer (Nano Drop Technologies) to ensure that only high-quality samples ($OD_{260}/_{280}$ = 1.8–2.2, an $OD_{260}/_{230} \geq 2.0$, an RNA integrity number (RIN) ≥ 6.5, 28S:18S > 1.0, > 1 μg) was used to construct sequencing library.

2.8.3 *Library preparation and sequencing*

RNA purification, reverse transcription, library construction and sequencing were performed at Shanghai Majorbio Bio-pharm Biotechnology Co., Ltd. (Shanghai, China) according to the

manufacturer's instructions (Illumina, San Diego, CA). The mRNA-seq transcriptome librariy was prepared following Illumina® Stranded mRNA Prep, Ligation from Illumina (San Diego, CA) using 1 μg of total RNA. Shortly, messenger RNA was isolated according to polyA selection method by oligo (dT) beads and then fragmented by fragmentation buffer firstly. Secondly double-stranded cDNA was synthesized using a SuperScript double-stranded cDNA synthesis kit (Invitrogen, CA) with random hexamer primers (Illumina). Then the synthesized cDNA was subjected to end-repair, phosphorylation and 'A' base addition according to Illumina's library construction protocol. Libraries were size selected for cDNA target fragments of 300 bp on 2% Low Range Ultra Agarose followed by PCR amplified using Phusion DNA polymerase (NEB) for 15 PCR cycles. After quantified by Qubit 4.0, paired-end RNA-seq sequencing library was sequenced with the NovaSeq X Plus sequencer (2 × 150 bp read length).

2.8.4 *Quality control and de novo assembly*

The raw paired end reads were trimmed and quality controlled by fastp with default parameters. Then clean data from the samples were used to do *de novo* assembly with Trinity. To increase the assembly quality, all the assembled sequences were filtered by CD-HIT and TransRate and assessed with BUSCO (Benchmarking Universal Single-Copy Orthologs). The assembled transcripts were searched against the NCBI protein nonredundant (NR), Clusters of Orthologous Groups of proteins (COG), and Kyoto Encyclopedia of Genes and Genomes (KEGG) databases using DIAMOND to identify the proteins that had the highest sequence similarity with the given transcripts to retrieve their function annotations and a typical cut-off *E*-values less than 1.0×10^{-5} was set. BLAST2GO program was used to get Gene Ontology (GO) annotations of unique assembled transcripts for describing biological processes (BP), molecular functions (MF) and cellular components (CC)[12].

2.8.5 *Differential expression analysis and functional enrichment*

To identify DEGs (differential expression genes) between two different samples/groups, the expression level of each transcript was calculated according to the transcripts per million reads (TPM) method. RSEM was used to quantify gene abundances[13]. Differential expression analysis was conducted using the DESeq2 package. Genes with $|\log_2 FC| \geq 1$ and FDR < 0.05 were defined as significantly DEGs. In addition, functional-enrichment analysis including GO and KEGG were performed to identify which DEGs were significantly enriched in GO terms and metabolic pathways at Bonferroni-corrected *P*-value < 0.05 compared with the whole-transcriptome background. GO functional enrichment and KEGG pathway analysis were carried out by Goatools and Python SciPy software, respectively.

2.9 Metabolomics methods

2.9.1 *Sample preparation*

Samples of PF, stored at −80 °C and collected at different time points, are first freeze-dried. The dried samples are then powdered and passed through a No. 3 sieve. Accurately weigh 0.1 g of this powder and place it into a clean conical flask. Add 50 mL of a 50% methanol aqueous solution to the flask, and dissolve the sample by vortexing and ultrasonicating for 30 min to prepare test solution.

2.9.2 *Chromatographic conditions*

The samples were analyzed by Acquity UPLC I-class system (Waters, USA) with a Waters ACQUITY UPLC BEH C18 column (2.1 mm × 100 mm, 1.7 μm). The mobile phase A was ultra-pure water with 0.1% formic acid, and mobile phase B was acetonitrile. The gradient elution procedure was: 0–3 min, 2%–2% B; 3–5 min, 2%–7% B; 5–15 min, 7%–21% B; 15–20 min, 21%–78% B; 20–21 min, 78%–85% B; 21–24 min, 85%–95% B; 24–26 min, 95%–95% B; 26–28 min, 95%–2% B, with the column temperature of 40 °C, the flow rate of 0.3 mL·min^{-1}, and the injection volume of 3 μL.

2.9.3 *Mass spectrometry conditions*

The electrospray ion source (ESI) and SYNAPT XS (Waters, USA) high-resolution time-of-flight mass spectrometry were used for analysis. PF is rich in polyphenolic compounds, which can generate stable precursor ions in negative ion mode with distinct characteristic fragment information, negative ion mode was used for detection, with a capillary voltage of 4 kV, a cone voltage of 50 V, and an ion source temperature of 150 °C. The atomizing gas is high-purity nitrogen gas, with a cone hole gas flow rate of 50 L·h^{-1}, a desolvation gas flow rate of 600 L·h^{-1}, and a desolvation temperature of 250 °C. Mass spectrometry data was collected in MS^E mode, with an ion scanning range of *m/z* 100–1,200. The low collision energy (LCE) was set to 10 eV, and the high collision energy (HCE) was set to 50 eV. Leu enkephalin (LE) was used for calibration during the data collection process. In negative ion mode, the precise *m/z* of LE $[M-H]^-$ is 554.2615.

2.9.4 *Metabolomics data processing and analysis*

The metabolomics data were collected using the MassLynx 4.1 workstation and processed using Progenesis QI (V2.0). The *m/z* tolerance parameter was set to less than 5 ppm for peak alignment and normalization to obtain basic compound information. The metabolomics data were then imported into Progenesis QI (V2.0) and EZinfo 3.0 for principal component analysis (PCA) and orthogonal partial least squares-discriminant analysis (OPLS-DA) to identify differential metabolites based on VIP and *P*-value criteria. Differential metabolites were further analyzed using MetaboAnalyst 4.0 (http://www.metaboanalyst.ca/) for metabolic pathway analysis.

3 Results and discussions

3.1 Changes in the drying stage of PE

Natural sun-drying induces pronounced morphological changes in PF. As illustrated in Fig. 1, the fruit epidermis gradually shrinks and turns brown or dark green, alongside the emergence of characteristic pale yellow granular protuberances. Dry-basis moisture content, defined as the water mass ratio relative to the absolute dry weight of the sample, was quantified to track dynamic moisture loss throughout processing. Additionally, natural drying sustains cellular integrity and viability for a limited time window. SEM observation of PF tissues collected at sequential drying time points revealed fully intact cellular structures at the early stage of sun exposure. With prolonged dehydration, continuous water depletion leads to cellular death and structural collapse. During the whole drying period, PF tissues are subjected to combined dehydration and thermal stress, which activates secondary metabolic pathways and drives the accumulation of bioactive secondary metabolites. Once cells lose viability, the pre-synthesized secondary metabolites undergo intricate chemical transformations including oxidation, hydrolysis

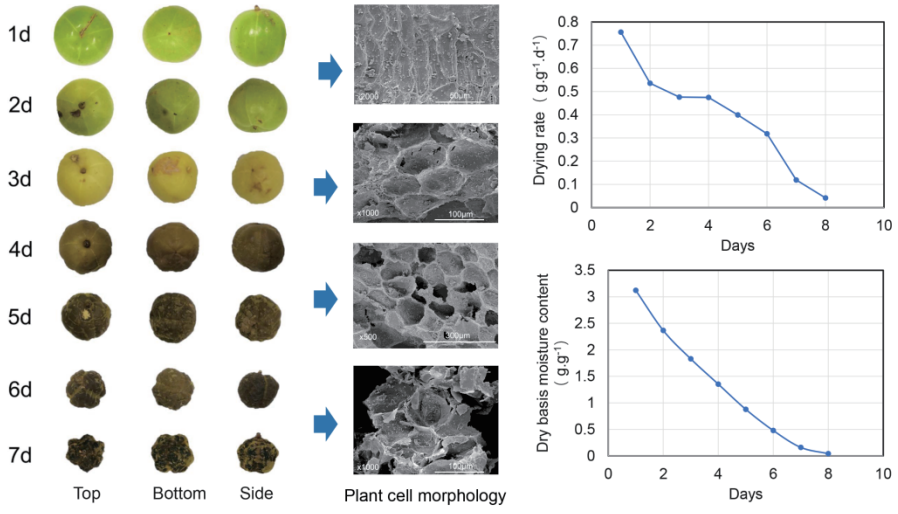

Figure 1 Dynamic variations in macroscopic morphology, cellular microstructure, and drying rate of PF across the entire natural sun-drying process.

and polymerization triggered by endogenous and exogenous stimuli, ultimately causing substantial shifts in the overall medicinal quality of PF.

3.2 Chemical component changes during the sun drying stage

In this research, HPLC fingerprinting was utilized to examine the pattern of compositional changes in PF, during the sun-drying process, with identification of the related constituents as depicted in Fig. 2A. A comparative assessment indicates that the longer the drying period, the lower the similarity in the HPLC profiles when compared to the samples from the first day of drying. It was observed that there were particularly pronounced changes in the levels of chebulagic acid, corilagin, gallic acid, epigallocatechin, chebulic acid, and ellagic acid, as shown in the corresponding detection results presented in Fig. 2B.

Our results demonstrated systematic dynamic fluctuations in the abundance of bioactive constituents throughout the natural sun-drying of PF. A subset of compounds including chebulic acid, epigallocatechin and corilagin declined to different degrees, whereas the contents of numerous other characteristic metabolites rose continuously. All these phytochemicals constitute the material basis for the pharmacological efficacy of PF. As a representative bioactive marker, chebulagic acid exerts dual inhibitory effects on two pro-inflammatory enzymes, 5-lipoxygenase (5-LOX) and cyclooxygenase-2 (COX-2), which largely accounts for the therapeutic potential of PF against multiple pharyngeal inflammatory disorders. Additionally, chebulagic acid has shown strong antiviral effects against hepatitis

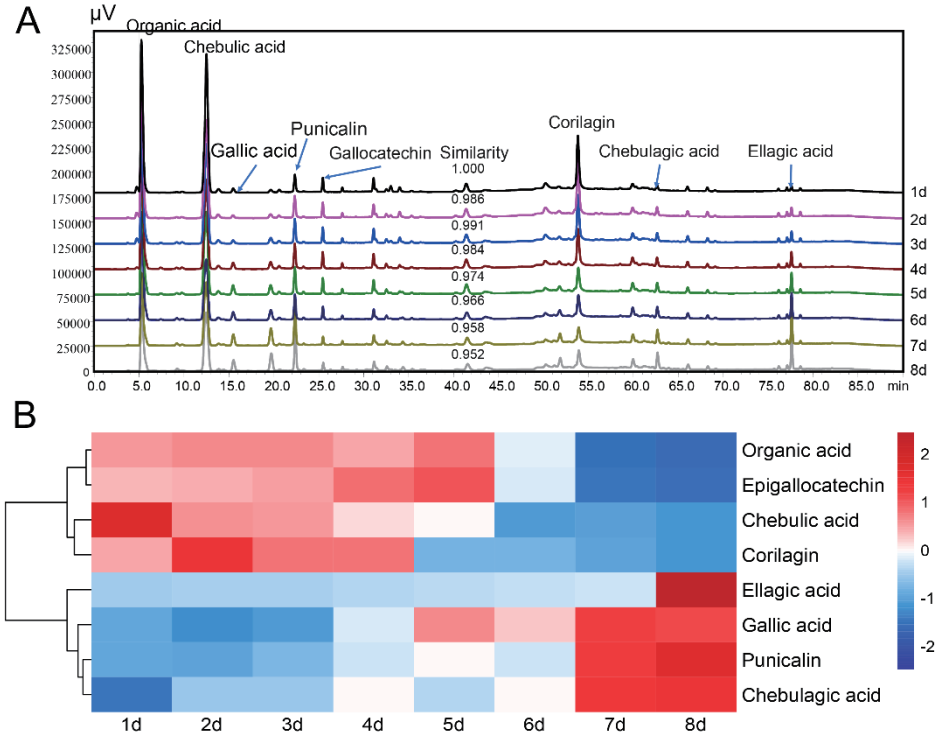

Figure 2 Variation patterns of major bioactive components in PF during natural sun-drying. (A) High-performance liquid chromatography (HPLC) characteristic fingerprints. (B) The abundance clustering heatmap of the major bioactive phytochemicals in PF harvested at sequential time points during natural sun-drying.

C and hepatoprotective capabilities. Corilagin, abundant in PF, exhibits a wide range of pharmacological activities, such as antitumor, antioxidant, anti-atherosclerotic, antithrombolytic, antihypertensive effects, and inhibitory actions against viruses, bacteria, and inflammation. The variations in the levels of these compounds may directly influence its clinical efficacy. The observed changes are likely due to the desiccation stress response of the plant material when subjected to dry and hot environmental conditions. To regulate the quality of the medicinal material, it is essential to first investigate the mechanisms underlying the formation of quality during the drying process, focusing on understanding the rules of quality transfer and the factors that influence them.

3.3 Transcriptomic results

3.3.1 Differential gene screening and annotation results before and after sun drying

Genes with differential expression can intuitively reflect the changes in life activities during BP and can provide reliable evidence for the research on the synthesis and metabolic mechanisms of plant secondary metabolites in this process. To explore the differences in gene expression in PF under different drying times, after obtaining the Read Counts data for genes/transcripts, it was standardized to per million base fragments to assess the expression levels of unigenes. Previous studies have demonstrated that tissue necrosis and severe RNA degradation occur in PF tissues after four days of dehydration, which renders subsequent transcriptome sequencing unfeasible. Accordingly, only samples collected within 0–4 days were subjected to transcriptomic analysis in this study. Considering that the samples include biological replicates, this study uses the DESeq2 software to perform comparative analysis of the transcriptome data of PF before and after drying. The differential gene screening criteria are: *P*-value < 0.05 and $|\log_2 FC| > 1$. The fold change threshold for up/down-regulation is set to 2. And the relevant results are presented in Fig. 3.

In Fig. 3A, transcriptome-based PCA analysis showed obvious separation between fresh and sun-dried PF samples. The volcano plot (Fig. 3B) visually reflected the correlation between false discovery rate and expression fold change, enabling rapid screening of genes with distinct expression patterns. In total, 2,515 significantly DEGs were screened out, including 1,261 upregulated and 1,254 downregulated genes. Venn diagram (Fig. 3C) analysis identified 26,457 shared unigenes/transcripts in the two groups, among which 13,762 transcripts were uniquely expressed in fresh samples (Group A) and 15,844 in sun-dried samples (Group B). As displayed in Fig. 3D, hierarchical clustering heatmap confirmed clear grouping separation between the two sample groups based on DEG expression profiles. These findings demonstrated that prolonged sun-drying induced profound transcriptomic reprogramming in PF fruits. The fruits actively regulated internal gene expression and physiological metabolism to adapt to external dehydration and thermal stress, thereby forming distinct transcriptional characteristics at different drying stages.

Subsequent functional classification was performed to explore the biological roles of these DEGs. As shown in Fig. 4A, GO annotation categorized all DEGs into biological process, CC and molecular function, and most annotated terms were closely linked to heat stress response. Within BP, cellular processes (1,512), metabolic processes (1,331), biological regulation (563), response to stimulus (379), localization (312) and CC organization (256) occupied the dominant proportions. For CC, most DEGs were

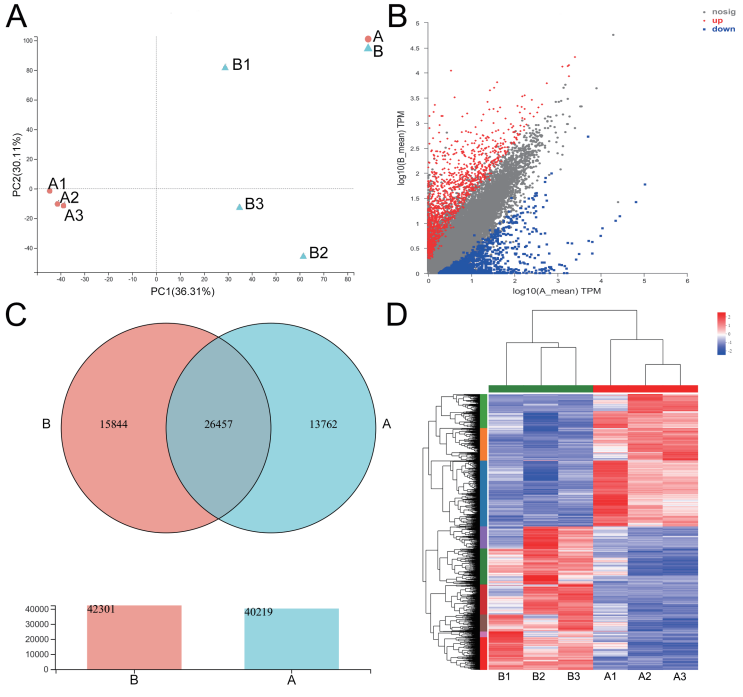

Figure 3 Global transcriptome differential expression statistics comparing fresh and sun-dried PF samples. Group A corresponds to fresh PF (pre-sun-drying), while Group B represents post-sun-drying PF. (A) PCA of all transcript expression profiles. (B) Volcano scatter plot illustrating differential expression magnitudes of all unigenes and transcripts. (C) Venn diagram showing shared and uniquely expressed unigenes/transcripts between two sample groups. (D) Hierarchical clustering heatmap of all significantly DEGs.Note: Every dot in panel 3B stands for an individual unigene or transcript. Gray dots denote genes/transcripts with non-significant expression changes. The absolute value of the horizontal coordinate reflects the fold change of gene expression, and points positioned closer to the horizontal zero line represent transcripts with weaker overall expression abundance.

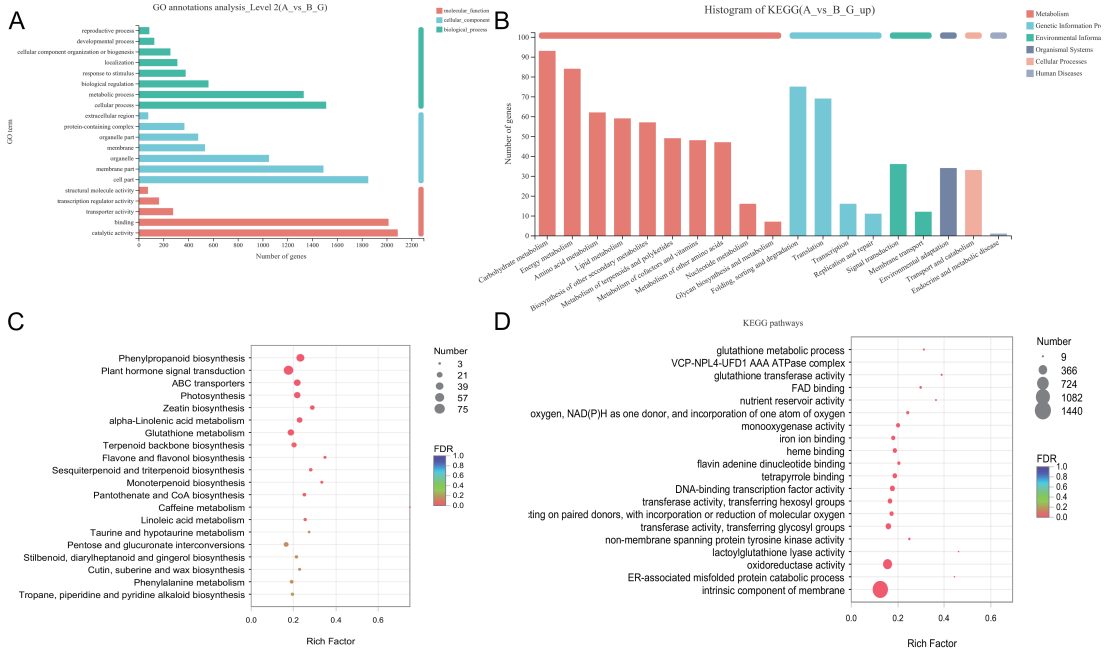

Figure 4 Functional classification and enrichment analyses of DEGs identified from fresh and sun-dried PF. (A) GO classification annotation of all DEGs. (B) KEGG pathway classification annotation of all DEGs. (C) Top significantly enriched GO functional terms for DEGs. (D) Top significantly enriched KEGG metabolic pathways for DEGs.

assigned to membrane-related structures (1,490), organelles (1,051), membrane parts (535), organelle components (480) and protein complexes (369). In terms of molecular function, catalytic activity (2,089) and binding activity (2,015) were the most enriched items, followed by transport activity (278).

Corresponding KEGG pathway annotation results are presented in Fig. 4B. The annotated DEGs were mainly distributed in metabolism, genetic information processing, environmental information processing, cellular processes and organismal systems. Metabolic pathways covered carbohydrate metabolism, energy metabolism, amino acid metabolism, lipid metabolism, secondary metabolite biosynthesis as well as terpenoid and polyketide metabolism. Genetic information processing pathways consisted of protein folding, sorting, degradation, DNA replication and repair, transcription and translation processes. Environmental information processing was mainly enriched in membrane transport and signal transduction pathways, while organismal system-related genes were primarily annotated in environmental adaptation pathways.

3.3.2 *GO enrichment analysis of DEGs*

Conduct GO annotation and functional enrichment analysis on the aforementioned DEGs to identify their main biological functional differences. When the corrected *P*-value (FDR) < 0.05, it is considered that this GO function is significantly enriched. The GO enrichment analysis of differential genes can observe the trend of changes during the drying process of PF, where the top 20 enriched GO terms are predominantly in the CC category, indicating that changes in molecular function categories have a significant impact on its heat stress at this stage.

Fig. 4C shows the enrichment of the three major functions (CC, BP, MF) annotated genes in the GO database (only shows GO enrichment with *P*-value < 0.05). In terms of CC, the most enriched in each group include the VCP-NPL4-UFD1 AAA ATPase complex and the intrinsic component of the membrane, which are strongly associated with cellular membrane activity. In terms of BP, the most enriched in A vs B are the glutathione metabolic process and the ER-associated misfolded protein catabolic process. In terms of MF, there is a noticeable increase in biological functions related to oxidative stress, such as glutathione transferase activity, FAD binding, nutrient reservoir activity, and oxidoreductase activity (acting on paired donors, with incorporation or reduction of molecular oxygen, NAD(P)H as one donor, and incorporation of one atom of oxygen).

As shown by the enrichment function from the GO database, most life activities during the drying process are strongly associated with the glutathione metabolic process. Glutathione is a well-recognized antioxidant within plants and plays an important role in enzyme activity and tissue antioxidant regulation. The size of the glutathione pool is strongly associated with the plant's resistance to various xenobiotics and environmental stress[14]. This indicates that under high-temperature stress, the various normal physiological processes of PF are inhibited, the reactive oxygen species (ROS) in the plant significantly increase, and the plant's heat stress mechanism is activated.

3.3.3 *KEGG enrichment analysis of DEGs*

The DEGs obtained from the comparison of different drying periods of PF were searched in the KEGG database, and enriched metabolic pathways were obtained. When the corrected *P*-value (FDR) < 0.05, it is considered that this KEGG pathway function is significantly enriched. Based on the aforementioned conditions, 5,663 DEGs were matched to 130 pathways, and 1,597 differential genes were enriched. As shown in Fig. 4D, the KEGG enrichment of differential genes before and after the drying of PF mainly involves pathways such as phenylpropanoid biosynthesis, plant hormone signal transduction, photosynthesis, ABC transporters, zeatin biosynthesis, α-linolenic acid metabolism, glutathione metabolism, terpenoid backbone biosynthesis, flavone and flavonol biosynthesis, sesquiterpenoid and triterpenoid biosynthesis, and monoterpenoid biosynthesis. Most of these pathways are involved in the biosynthesis of important secondary metabolites of PF, such as the phenylpropanoid pathway involved in polyphenol synthesis, flavonoid synthesis pathways, α-linolenic

acid metabolism, and terpenoid synthesis. These secondary metabolites can alleviate the high-temperature stress from the external environment on the plant tissues of PF, enhance the plant's stress resistance, and are also key factors in promoting the formation and improvement of the quality of PF medicinal materials.

The enrichment analysis of DEGs during the drying process of PF involves multiple heat stress response pathways, playing an important regulatory role in the response to high-temperature stress through pathways such as ROS clearance, DNA repair, and secondary metabolite synthesis. The phenylpropanoid pathway, flavonoid biosynthesis pathway, and terpenoid biosynthesis pathway alleviate oxidative stress caused by high-temperature stress, and their metabolic products are involved in the stress response to high-temperature stress. Notably, the phenylpropanoid biosynthesis pathway, which is the pathway for the synthesis of polyphenolic compounds in plants, ends with the product 4-coumaroyl-CoA, which can further generate a variety of plant polyphenolic products that play roles in antioxidant, UV radiation resistance, and drought resistance under external heat stress conditions. Since polyphenolic compounds are characteristic components of PF, this may be an important pathway for the formation and improvement of PF quality during the sun-drying period.

3.3.4 Analysis of biosynthetic metabolic pathways involving DEGs

The phenylpropanoid biosynthetic pathway is an important secondary metabolic product synthesis pathway in plants, with the synthesis of plant tannins being one of its branch pathways. Starting with L-phenylalanine as the substrate, it provides the material basis for a variety of subsequent phenylpropanoid metabolites, including flavonoids, phenols, and lignin. Based on the analysis of the PF transcriptome database annotation results, 53 genes were enriched in the biosynthesis of the polyphenolic skeleton, involving enzymes such as phenylalanine ammonia-lyase (PAL), 4-coumarate-CoA ligase (4CL), cinnamoyl-CoA reductase (CCR), cinnamyl-alcohol dehydrogenase (CAD), shikimate O-hydroxycinnamoyltransferase (HCT), coniferyl-aldehyde dehydrogenase (REF1), and caffeoyl-CoA O-methyltransferase (E2.1.1.104). The enriched DEGs had 31 upregulated and 22 downregulated in comparison A vs B, overall showing an upregulation trend, indicating that the synthesis of secondary metabolites such as phenols, lignins, and flavonoids is enhanced during the drying process.

The biosynthetic pathway of flavonoids and flavonols is another important secondary metabolic product synthesis pathway in PF, with the secondary metabolites it produces being an important class of active components in PF. Based on the analysis of the PF transcriptome database annotation results, a total of 8 differential genes were enriched in the biosynthesis of flavonoids and flavonols, involving enzymes such as flavonol-3-*O*-L-rhamnoside-7-*O*-glucosyltransferase (UGT73C6), flavonol-3-*O*-glucoside/galactoside glucosyltransferase (FG3), flavonol-3-*O*-glucoside L-rhamnosyltransferase (FG2), flavonoid 3'-monooxygenase (CYP75B1), and flavonoid 3',5'-hydroxylase (CYP75A). The enriched DEGs had 8 upregulated and 0 downregulated in comparison A vs B, indicating that the biosynthesis of flavonoid compounds in PF is more active during the drying process.

The terpenoid backbone biosynthetic pathway is another important secondary metabolic product synthesis pathway in PF and an important class of active components. It can synthesize precursors of terpenoid components in PF, such as phyllaemblic acid and its derivatives phyllaemblic acid methyl ester, phyllaemblicin A, phyllaemblicin B, phyllaemblicin C, phyllaemblic acid B, and lupeol, which possess strong antiviral activity. Based on the analysis of the PF transcriptome database annotation results, a total of 23 differential genes were enriched in the pathways. Among them, 18 were upregulated and 5 were downregulated in comparison A vs B, indicating that this pathway is more active during the drying process of PF, with an upward trend in biosynthesis. The main enzymes involved include acetyl-CoA C-acetyltransferase (ACAT), 1-deoxy-D-xylulose-5-phosphate synthase (DXS), hydroxymethylglutaryl-CoA reductase (HMGCR), 2-C-methyl-D-erythritol 4-phosphate cytidylyltransferase (ISPD), mevalonate kinase (MVK), 2-C-methyl-D-erythritol 2,4-cyclodiphosphate synthase (ISPF), and (*E*)-4-hydroxy-3-methylbut-2-enyl-diphosphate synthase (GcpE).

3.4 Metabolomics results

3.4.1 Multivariate statistical analysis results

To further confirm the main biosynthetic pathways involved in its drying process, this study utilized a metabolomics approach based on UPLC-QTOF-MS to investigate the metabolic pathways during the drying period of PF. Multivariate statistical analysis was employed in the experiment to identify differential metabolites. Starting from the sample taken on the first day of drying, samples at different drying time points could be distinctly differentiated in PCA result (Fig. 5A), indicating that the overall chemical composition is undergoing significant changes. Additionally, the relatively small differences between sample groups suggest good biological replicates of the samples. At the same time, sample A has the greatest Euclidean distance from other samples, indicating the largest difference. Over time, these differences diminish, suggesting that compositional changes are more pronounced in the early stages of drying compared to the later stages.

Supervised partial least squares discrimination analysis (PLS-DA) was used to analyze the metabolomic data. By comparing the samples from the first and last day, it was found that Group A and Group K (drying samples of first and last day) can be distinctly differentiated, with significant differences in metabolites (Fig. 5B, R^2X = 0.997, R^2Y = 0.999, Q^2 = 0.99). This indicates that the model is reliable, with good internal validation and predictive capabilities. To prevent overfitting, internal validation tests were conducted. With 100 permutations set, the results shown (Fig. 5C) indicate R^2 = (0.0, 0.249), Q^2 = (−0.0, −0.247), which suggests that the model does not suffer from overfitting. After that, S-plot was further used to identify differential chemical markers, with the screening conditions set to VIP > 1 and P < 0.05 for selection. In the S-plot (Fig. 5D) result, the farther the variables deviate from the origin, the greater the difference. Based on the accurate *m/z* of the ion characteristic metabolites and the fragment characteristics (predicted ion fragment matching), and compared with the reference substance, a total of 58 characteristic metabolites were identified in the samples (Table 2), mainly consisting of phenolic acids, tannins, and flavonoids.

3.4.2 Differential metabolite analysis

In the study, cluster heatmaps were used to illustrate the variation patterns and analyze the trend of differential metabolite markers among various groups, and the result is shown in Fig. 5E. From the cluster heatmap analysis, it can be seen that during the

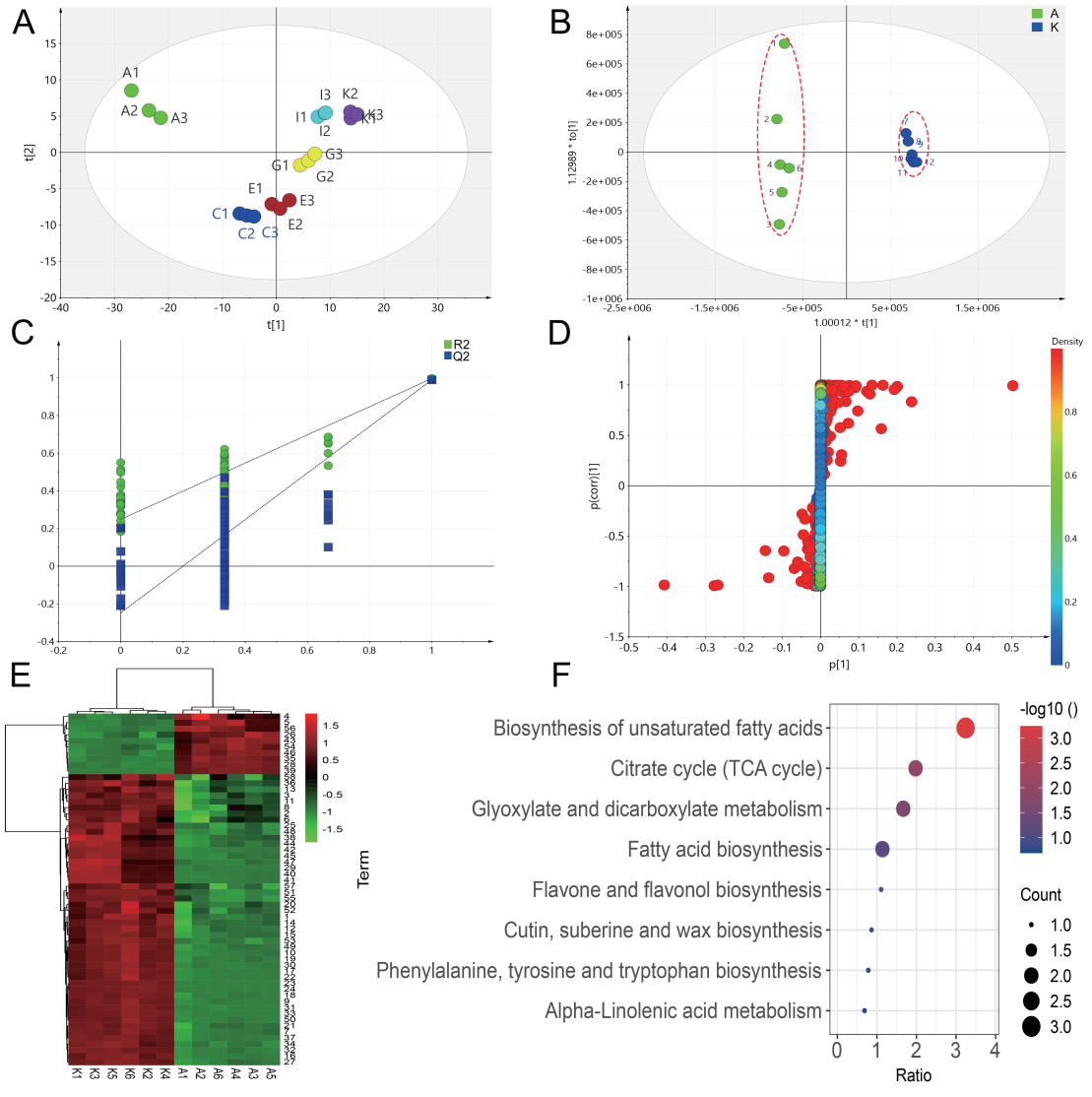

Figure 5 Multivariate statistical analysis of metabolomic data from PF samples collected at different sun-drying time points. Sample A denotes fresh PF collected on day 1 of drying, and Sample K represents PF collected on the final day of the 11-day drying period. (A) PCA of all metabolite profiles across drying stages. (B) Orthogonal partial least squares discriminant analysis (OPLS-DA) distinguishing day 1 and day 11 metabolites. (C) Permutation test for internal validation of the OPLS-DA model. (D) S-plot screening characteristic differential metabolites with significant abundance shifts. (E) Abundance clustering heatmap of all annotated differential metabolites. (F) KEGG pathway enrichment analysis of screened differential metabolites.

Table 2 Identification results of differential metabolites

No	*Rt*	*m/z*	Compounds name	Adduct	Molecular formula	Error (ppm)
1	0.6	191.018,9	D-Glucaro-1,4-lactone	M-H	$C_6H_8O_7$	−4.18
2	0.65	361.039,9	2-*O*-Galloylgalactaric acid	M-H	$C_{13}H_{14}O_{12}$	−3.64
3	0.67	331.066,5	*β*-Glucogallin	M-H	$C_{13}H_{16}O_{10}$	−1.73
4	0.68	701.047,9	Gossypetin 8-glucuronide 3-glucoside	M+Cl	$C_{27}H_{28}O_{19}$	−0.89
5	0.76	503.047,5	3,4-Dihydroxy-5-[3-hydroxy-4-methoxy-5-(2,3,4,5-tetrahydroxybenzoyloxy)benzoyloxy]benzoic acid	M-H	$C_{22}H_{16}O_{14}$	1.54
6	0.77	1,139.058,6	Sanguiin H2	M+Cl	$C_{48}H_{32}O_{31}$	−3.20
7	0.86	337.018,9	(+)-Chebulic acid	M-H_2O-H	$C_{14}H_{12}O_{11}$	−3.53
8	0.89	513.051,5	6-{3-[(5-Carboxy-2,3-dihydroxyphenoxy)carbonyl]-2,5,6-trihydroxyphenoxy}-3,4,5-Trihydroxyoxane-2-carboxylic acid	M-H	$C_{20}H_{18}O_{16}$	−1.31
9	0.94	343.029,8	2-*O*-Galloyl-1,4-galactarolactone	M-H	$C_{13}H_{12}O_{11}$	−2.63
10	0.94	191.018,9	Citric acid	M-H	$C_6H_8O_7$	−4.53
11	1.21	513.051,1	3,4,5-Trihydroxy-6-[2,4,5-trihydroxy-3-(3,4,5-trihydroxybenzoyloxy)benzoyloxy]oxane-2-carboxylic acid	M-H	$C_{20}H_{18}O_{16}$	−2.07
12	1.26	331.066,4	*β*-Glucogallin	M-H_2O-H	$C_{13}H_{16}O_{10}$	−3.02

(Continued)

No	*Rt*	*m/z*	Compounds name	Adduct	Molecular formula	Error (ppm)
13	1.26	271.045,1	Prephenate	M+FA-H	$C_{10}H_{10}O_6$	−3.92
14	1.28	327.034,8	3,4,5-Trihydroxy-6-(3,4,5-trihydroxybenzoyloxy)oxane-2-carboxylic acid	M-H_2O-H	$C_{13}H_{14}O_{11}$	−2.78
15	1.46	271.045,0	Fukiic acid	M-H	$C_{11}H_{12}O_8$	−3.44
16	1.51	191.018,7	Galactaric acid	M-H_2O-H	$C_6H_{10}O_8$	−4.70
17	1.73	375.055,8	6-Methyl 2-galloylgalactarate	M-H	$C_{14}H_{16}O_{12}$	−2.95
18	2.07	343.029,7	2-*O*-Galloyl-1,4-galactarolactone	M-H	$C_{13}H_{12}O_{11}$	−2.77
19	2.07	191.019,0	Isocitric acid	M-H	$C_6H_8O_7$	−3.83
20	2.20	301.055,8	Pyrogallol-2-*O*-glucuronide	M-H	$C_{12}H_{14}O_9$	−2.32
21	2.31	513.051,6	3,4,5-Trihydroxy-6-[2,3,4-trihydroxy-5-(3,4,5-trihydroxybenzoyloxy)benzoyloxy]oxane-2-carboxylic acid	M-H	$C_{20}H_{18}O_{16}$	−1.21
22	2.37	375.055,9	6-Methyl 2-galloylgalactarate	M-H	$C_{14}H_{16}O_{12}$	−2.60
23	3.19	237.060,6	Quinic acid	M+FA-H	$C_7H_{12}O_6$	−4.92
24	5.29	389.071,6	Dimethyl 2-galloylgalactarate	M-H	$C_{15}H_{18}O_{12}$	−2.42
25	5.62	343.029,6	2-*O*-Galloyl-1,4-galactarolactone	M-H	$C_{13}H_{12}O_{11}$	−3.16
26	5.82	183.029,1	Succinylacetoacetate	M-H_2O-H	$C_8H_{10}O_6$	−3.74
27	5.91	633.072,4	Corilagin	M-H	$C_{27}H_{22}O_{18}$	−1.49
28	6.15	761.135,6	3'-Galloylprodelphinidin B2	M-H	$C_{37}H_{30}O_{18}$	−0.42
29	6.47	665.062,2	6-{4-[(3-Carboxy-2,5,6-trihydroxyphenoxy)carbonyl]-2-hydroxy-6-(3,4,5-trihydroxybenzoyloxy)phenoxy}-3,4,5-trihydroxyoxane-2-carboxylic acid	M-H	$C_{27}H_{22}O_{20}$	−1.40
30	6.50	483.078,2	1,6-Digalloyl-*β*-D-glucopyranose	M-H	$C_{20}H_{20}O_{14}$	0.39
31	6.86	625.104,9	Amritoside	M-H	$C_{26}H_{26}O_{18}$	0.35
32	7.02	343.029,8	3-*O*-Galloyl-1,4-galactarolactone	M-H	$C_{13}H_{12}O_{11}$	−2.52
33	7.44	631.056,9	6-[5-({5-[(5-Carboxy-2,3-dihydroxyphenoxy)carbonyl]-2,3-dihydroxyphenoxy}carbonyl)-2,3-dihydroxyphenoxy]-3,4,5-trihydroxyoxane-2-carboxylic acid	M-H_2O-H	$C_{27}H_{22}O_{19}$	−1.28
34	7.78	485.047,0	Myricetin 3-arabinoside	M+Cl	$C_{20}H_{18}O_{12}$	−4.87
35	8.10	457.075,8	Diosmetin 7-*O*-*β*-D-glucuronopyranoside	M-H_2O-H	$C_{22}H_{20}O_{12}$	−3.94
36	8.83	473.035,4	*m*-Trigallic acid	M-H	$C_{21}H_{14}O_{13}$	−1.69
37	8.83	635.088,5	1,3,4-Trigalloyl-*β*-D-glucopyranose	M-H	$C_{27}H_{24}O_{18}$	−0.80
38	8.83	1,105.100,6	Syzyginin A	M-H	$C_{48}H_{34}O_{31}$	−0.49
39	9.32	729.145,6	*ent*-Epicatechin-(4*α*→8)-ent-epicatechin 3'-gallate	M-H	$C_{37}H_{30}O_{16}$	−0.66
40	9.57	1,103.085,4	Sanguiin H2	M-H	$C_{48}H_{32}O_{31}$	−0.08
41	9.79	1,105.100,8	Syzyginin A	M-H_2O-H	$C_{48}H_{34}O_{31}$	−0.62
42	10.43	300.998,2	Ellagic acid	M-H	$C_{14}H_6O_8$	−2.61
43	10.91	441.081,9	3,4,5-Trihydroxy-6-[(7-hydroxy-5-methoxy-4-oxo-2-phenyl-4H-chromen-6-yl)oxy]oxane-2-carboxylic acid	M-H_2O-H	$C_{22}H_{20}O_{11}$	−1.80
44	10.95	785.084,0	Tercatain	M-H	$C_{34}H_{26}O_{22}$	−0.42
45	11.02	1,103.084,5	Sanguiin H2	M-H	$C_{48}H_{32}O_{31}$	−0.89
46	11.17	441.139,2	3,4,5-Trihydroxy-6-({2-hydroxy-3-[4-hydroxy-3-(4-hydroxy-3-methylbut-2-en-1-yl)phenyl]propanoyl}oxy)oxane-2-carboxylic acid	M-H	$C_{20}H_{26}O_{11}$	−2.34
47	11.48	937.093,6	Tellimagrandin II	M-H	$C_{41}H_{30}O_{26}$	−1.80
48	11.59	309.097,1	(*E*)-2-*O*-Cinnamoyl-*β*-D-glucopyranose	M-H	$C_{15}H_{18}O_7$	−2.78
49	12.85	447.092,6	Quercitrin	M-H	$C_{21}H_{20}O_{11}$	−1.56
50	13.42	461.071,8	Kaempferol 3-glucuronide	M-H	$C_{21}H_{18}O_{12}$	−1.60
51	14.49	431.097,7	Kaempferol 3-*O*-*α*-L-rhamnofuranoside	M-H	$C_{21}H_{20}O_{10}$	−1.62
52	16.22	461.108,5	2-Cinnamoyl-1-galloyl-*β*-*D*-glucopyranose	M-H	$C_{22}H_{22}O_{11}$	−1.04
53	16.52	613.119,3	2-Cinnamoyl-1,6-digalloyl-*β*-*D*-glucopyranose	M-H	$C_{29}H_{26}O_{15}$	−1.04
54	16.74	723.192,8	4-[2-(3,4-Dihydroxyphenyl)-3,5,7-trihydroxy-3,4-dihydro-2H-1-benzopyran-8-yl]-2-(3-hydroxyphenyl)-6-[3,4,5-trihydroxy-6-(hydroxymethyl)oxan-2-yl]-3,4-dihydro-2H-1-benzopyran-3,5,7-triol	M-H	$C_{36}H_{36}O_{16}$	−0.30
55	20.87	295.226,8	Octadecanedioic acid	M-H_2O-H	$C_{18}H_{34}O_4$	−3.34
56	21.37	277.216,6	*α*-Linolenic acid	M-H	$C_{18}H_{30}O_2$	−2.44
57	22.71	281.247,5	Oleic acid	M-H	$C_{18}H_{34}O_2$	−3.75
58	23.75	283.263,4	Stearic acid	M-H	$C_{18}H_{36}O_2$	−2.93

drying stage, the content of most active components such as polyphenols, flavonoids, and phenolic acids significantly increases, enhancing the quality of the medicinal material. The decrease in the content of a few components may be related to component transformation.

3.4.3 KEGG functional annotation and enrichment analysis of differential metabolites

All annotated differential metabolites were matched with corresponding HMDB identifiers and subsequently submitted to MetaboAnalyst 5.0 for pathway enrichment analysis. As illustrated in Fig. 5F, the perturbed metabolic cascades predominantly covered unsaturated fatty acid biosynthesis, the tricarboxylic acid (TCA) cycle, glyoxylate and dicarboxylate metabolism, *de novo* fatty acid synthesis, flavone and flavonol biosynthesis, cutin–suberin–wax biosynthesis, phenylalanine/tyrosine/tryptophan biosynthesis, and α-linolenic acid metabolism. Such enrichment profiles exhibited strong consistency with the transcriptomic pathway enrichment outcomes, jointly corroborating the widespread metabolic reprogramming triggered by sun-drying stress in PF fruit tissues. Collectively, these metabolic shifts constitute a coordinated adaptive strategy deployed by PF to withstand combined dehydration and thermal stress during natural sun exposure.Pathways governing unsaturated fatty acid and α-linolenic acid metabolism were significantly perturbed as a vital membrane-protective adaptive mechanism. Severe drought and solar radiation trigger massive ROS accumulation that easily causes lipid peroxidation and membrane damage. To counteract such oxidative injury, PF remodels membrane lipid composition by elevating polyunsaturated fatty acid levels. Higher lipid unsaturation stabilizes membrane structure and fluidity, alleviating oxidative degradation of organelle membranes and retaining basic physiological metabolism in intact fruit cells within the early drying period.

Drying stress initiates a complete regulatory cascade centered on phenylpropanoid and flavonoid biosynthesis, which is tightly linked to the quality formation of PF. Upon sensing thermal and dehydrative stimuli, stress signaling pathways trigger transcriptional upregulation of key rate-limiting enzyme genes in these two secondary metabolic branches[14]. The activated enzymes accelerate the conversion of carbon precursors to phenolic intermediates, which undergo continuous hydroxylation, glycosylation and esterification to gradually accumulate gallic acid, chebulagic acid, ellagic acid, punicalagin and other characteristic polyphenols and tannins, the core bioactive substances determining the medicinal efficacy of PF.

Central carbon energy metabolism, lipid metabolism and polyphenol-based secondary metabolism coordinate synergistically to build a multi-level antioxidant defense system, and this collaborative regulation is further supported by existing research on *Arabidopsis thaliana*, which has proven that flavonoid and phenolic accumulation effectively improves plant drought resistance. Central carbon metabolism supplies persistent carbon substrates for defensive metabolite synthesis, lipid remodeling maintains cellular membrane integrity to sustain metabolic activity, and accumulated flavonoids and tannins eliminate excess ROS as non-enzymatic antioxidants. Collectively, sun-drying stress activates interconnected primary and secondary metabolic networks as a self-protective response; the coordinated reinforcement of carbon supply, membrane protection and polyphenol biosynthesis continuously enriches signature active constituents and ultimately elevates the overall medicinal quality of PF.

3.5 Transcriptome and metabolome integration analysis

Combined transcriptomic and metabolomic datasets were integrated to systematically dissect the regulatory linkages between core functional enzyme genes and differential metabolites during PF sun-drying, *via* joint KEGG pathway mapping and gene-metabolite correlation network construction. Joint KEGG mapping revealed consistent enrichment of three pivotal secondary metabolic cascades shared by both omics layers: Phenylpropanoid biosynthesis, flavonoid and flavonol biosynthesis, and terpenoid backbone biosynthesis, alongside primary metabolic routes including α-linolenic acid metabolism and the TCA cycle.

Within the phenylpropanoid pathway, rate-limiting enzyme genes *PAL*, *4CL*, *HCT*, and *CAD* exhibited pronounced upregulation after sun-drying, and their expression levels displayed strong positive correlations with gallic acid, corilagin, chebulagic acid, and ellagic acid. These tannin-derived polyphenols continuously accumulated under drought and heat stress, which could be attributed to the transcriptional activation of upstream phenylpropanoid structural genes that supplied sufficient phenolic precursors for hydrolyzable tannin biosynthesis. For flavonoid and flavonol biosynthesis, all eight enriched DEGs encoding glycosyltransferases and cytochrome P450 hydroxylases (e.g., *CYP75A*, *CYP75B1*, *UGT73C6*) were significantly upregulated, showing tight positive correlations with flavonol glycosides and punicalagin; these enzyme genes govern the hydroxylation and glycosylation modifications of flavonoid skeletons, facilitating the production and storage of UV- and stress-resistant flavonoid metabolites.

In the terpenoid backbone biosynthesis pathway, 18 upregulated enzyme genes including *DXS*, *HMGCR*, and *MVK* were strongly correlated with terpenoid bioactive markers such as phyllaemblic acid derivatives, which confer antiviral and hepatoprotective properties to PF. Meanwhile, stress-responsive primary metabolic genes involved in glutathione metabolism and α-linolenic acid metabolism were positively associated with unsaturated fatty acid metabolites, which serve as signal molecules to activate downstream antioxidant and stress defense cascades.

Notably, a small subset of metabolites (e.g., chebulinic acid, catechin gallate) declined throughout sun-drying, and their variation trends were negatively correlated with most key secondary metabolic enzyme genes. This inverse correlation indicated that these compounds act as intermediate precursors and are continuously transformed into high-value polyphenolic end-products under sustained desiccation and thermal stimuli.

4 Conclusion

Metabolomic analysis of PF chemical constituents revealed variable changes in the abundance of bioactive compounds during sun drying. Specifically, key functional components including gallic acid, corilagin, chebulagic acid, ellagic acid, and punicalagin were elevated to varying degrees, whereas a small subset of metabolites (e.g., organic acids, chebulinic acid, and catechin gallate) displayed a declining trend. Such metabolic alterations are presumably attributed to the activation and reprogramming of component biosynthesis, transformation, and degradation processes in PF tissues under drought and thermal stress during

sun drying.

Transcriptomic and metabolomic evidence further indicated that sun-drying stress potentially activates multiple secondary metabolic pathways in PF, prominently including phenylpropanoid biosynthesis, flavonoid and flavonol synthesis, and terpenoid metabolism, which collectively govern the accumulation of polyphenolic bioactive substances[2]. Additionally, primary metabolic pathways such as α-linolenic acid metabolism, linoleic acid metabolism, and amino acid metabolism were also differentially modulated, consistent with the observed metabolomic profiles.

Drying approaches are critical external factors shaping the macroscopic traits, physical properties, and chemical metabolic profiles of PF medicinal materials[8]. During the initial 3–4 days of sun drying, PF tissue cells remain morphologically intact. Distinct from rapid artificial drying modes, the gradual dehydration and mild thermal stress imposed by natural sun drying may trigger active stress responses in viable PF cells, thereby driving adaptive metabolic reprogramming and dynamic changes in active ingredient contents.

Current quality standards permit multiple drying strategies for PF, including oven drying, sun drying, and freeze drying. Rather than asserting the absolute superiority of sun drying, the present study proposes a potential stress-driven quality formation mechanism: The drought and thermal stimuli occurring during natural sun drying may serve as key regulatory factors modulating the metabolic characteristics and medicinal quality of PF. This work offers a novel perspective for understanding the quality formation mechanism of PF, and provides theoretical references for the optimization of post-harvest processing protocols and the improvement of quality evaluation standards for PF.

Data availability

All data needed to support the conclusions in the paper are presented in the manuscript and/or the Electronic Supplementary Material. Additional data related to this paper may be requested from the corresponding author upon request.

Conflicts of interest

The authors declare that there are no conflicts of interest in this work.

Acknowledgements

None.

Funding

This study was supported by grants from the National Natural Science Foundation of China (82304871); Sichuan Science and Technology Program (2024YFFK0185); Research Fund Project Grant for Sichuan Nursing Vocational College (2024ZRY12).

Author contribution statement

Hao-Zhou Huang and Meng-Qi Li: Methodology, data curation, writing-original draft preparation. San-Hu Fan and Tai-Gang Mo: Data collection and analysis of odor analysis. Jun-Zhi Lin: Sample collection and pretreatment. Li Han and Ding-Kun Zhang: Conceptualization, supervision, validation, writing-reviewing and editing.

Informed consent

Not applicable

Ethics statement

Not applicable.

Use of AI statement

None.

References

[1] Variya, B. C., Bakrania, A. K., Patel, S. S. *Emblica officinalis* (Amla): A review for its phytochemistry, ethnomedicinal uses and medicinal potentials with respect to molecular mechanisms. *Pharmacological Research*, **2016**, 111: 180–200. https://doi.org/10.1016/j.phrs.2016.06.013

[2] Agati, G., Brunetti, C., Di Ferdinando, M., et al. Functional roles of flavonoids in photoprotection: New evidence, lessons from the past. *Plant Physiology and Biochemistry*, **2013**, 72: 35–45. https://doi.org/10.1016/j.plaphy.2013.03.014

[3] Li, M. Q., Yu, Q., Li, G. F., et al. *Phyllanthus emblica* fruits: A polyphenol-rich fruit with potential benefits for oral management. *Food & Function*, **2023**, 14: 7738–7759. https://doi.org/10.1039/d3fo01671d

[4] Huang, H., Li, M., Tan, Q., et al. The impact of thermal extraction on the quality of *Phyllanthus emblica* Linn. fruit: A systematic study based on compositional changes. *Arabian Journal of Chemistry*, **2023**, 16: 104562. https://doi.org/10.1016/j.arabjc.2023.104562

[5] Mahajan, S., Bisht, M. S., Chakraborty, A., et al. Genome of *Phyllanthus emblica*: The medicinal plant Amla with super antioxidant properties. *Frontiers in Plant Science*, **2023**, 14: 1210078. https://doi.org/10.3389/fpls.2023.1210078

[6] Huang, H. Z., Tan, P., Li, M. Q., et al. Quality analysis combined with mass spectrometry imaging reveal the difference between wild and cultivated *Phyllanthus emblica* Linn.: From chemical composition to molecular mechanism. *Arabian Journal of Chemistry*, **2022**, 15: 103790. https://doi.org/10.1016/j.arabjc.2022.103790

[7] Huang, H. Z., Li, M. Q., Li, G. F., et al. Dynamic changes in chemical composition and microbial community characteristics during pile-fermentation process of *Phyllanthus emblica* Linn. fruit. *Arabian Journal of Chemistry*, **2023**, 16: 105166. https://doi.org/10.1016/j.arabjc.2023.105166

[8] Su, X. Y., Wu, Y. J., Li, Y., et al. Effect of different post-harvest processing methods on the chemical constituents of *Notopterygium franchetii* by an UHPLC-QTOF-MS-MS metabolomics approach. *Molecules*, **2019**, 24: 3128. https://doi.org/10.3390/molecules24173128

[9] Li, S. L., Yan, R., Tam, Y. K., et al. Post-harvest alteration of the main chemical ingredients in *Ligusticum chuanxiong* Hort. (Rhizoma Chuanxiong). *Chemical and Pharmaceutical Bulletin*, **2007**, 55: 140–144. https://doi.org/10.1248/cpb.55.140

[10] Hartmann, T. From waste products to ecochemicals: Fifty years research of plant secondary metabolism. *Phytochemistry*, **2007**, 68: 2831–2846. https://doi.org/10.1016/j.phytochem.2007.09.017

[11] Harui, A., Maruyama, S., Segawa, Y., et al. Effect of *Saccharina japonica* intake on blood pressure and gut microbiota composition in spontaneously hypertensive rats. *Microorganisms*, **2024**, 12: 556. https://doi.org/10.3390/microorganisms12030556

[12] Conesa, A., Götz, S., García-Gómez, J. M., et al. Blast2GO: A universal tool for annotation, visualization and analysis in functional genomics research. *Bioinformatics*, **2005**, 21: 3674–3676. https://doi.org/10.1093/bioinformatics/bti610

[13] Li, B., Dewey, C. N. RSEM: Accurate transcript quantification from

RNA-Seq data with or without a reference genome. *BMC Bioinformatics*, **2011**, 12: 323. https://doi.org/10.1186/1471-2105-12-323

[14] Wang, N., Liu, W. J., Yu, L., et al. Heat shock factor A8a modulates flavonoid synthesis and drought tolerance. *Plant Physiology*, **2020**, 184: 1273–1290. https://doi.org/10.1104/pp.20.01106